Journal of Applied Fluid Mechanics, Vol. 9, No. 1, pp. 333-341, 2016.
Available online at www.jafmonline.net, ISSN 1735-3572, EISSN 1735-3645.
DOI: 10.18869/acadpub.jafm.68.224.24003

Numerical Study of Water Production from Compressible Moist-Air Flow

S. Hamidi [1†] and M. J. Kermani [2]

[1]*Department of Mechanical Engineering, Sanandaj Branch, Islamic Azad University, Sanandaj, Iran*
[2]*Department of Mechanical Engineering, Amirkabir University of Technology, Tehran, Iran*
†*Corresponding Author Email:sabaah_hamidi@yahoo.com*

(Received August 23, 2014; accepted January 30, 2015)

ABSTRACT

In this research a numerical study of water production from compressible moist-air flow by condensing of the vapor component of the atmospheric air through a converging-diverging nozzle is performed. The atmospheric air can be sucked by a vacuum compressor. The geographical conditions represent a hot and humid region, for example Bandar Abbas, Iran, with coordinates, 27^0 11' N and 56^0 16' E and summer climate conditions of about 40℃and relative humidity above 80%. Parametric studies are performed for the atmospheric-air temperature between, 40℃ to 50℃, and relative humidity between49.6% to 100.%. For these ranges of operating conditions and a nozzle with the area ratio of 1.17, the liquid mass flow rates falls in the range 0.272 to 0.376 kg/s. The results show that, the energy consumed by the compressor for production 1 kg of water will be 1.279 kWh. The price of 1 kWh is 372 Rials, therefore the price for the production of 1 kg liquid water will be 475.8 Rials, therefore, the scheme is economically suitable.

Keywords: Water Production; Condensation of Moist-Air; Equilibrium thermodynamic; Roe's scheme.

1. INTRODUCTION

The traditional sources of water in many regions of the world are surface water, ground water and rain water. Atmospheric air usually includes water vapor. One of the recent methods of water production is by condensation of the steam portion of the atmospheric air. Some studies are performed for water production from atmospheric air. Atmospheric water vapor processing (AWVP) is a new technology in which, water can be extracted from moist atmospheric air by phase change from vapor to liquid (Wahlgren, (2001)). Three methods have been described in the AWVP types, (a) heat pumps are used to cool surfaces so water vapor can be condensed and collected, (b) concentration of the water vapor by desiccants where water molecules are absorbed in a liquid or adsorbed on a solid, and (c) inducing convection currents in a tall tower structure, expanding the air, which transforms some of the energy in the air into work, thus cooling the air below its dew-point and causing some of the water vapor to condense into liquid water. Our numerical study in this paper is similar to method (c).

A scheme for large-scale dew collection as a source of fresh water production is studied by Rajvanshi (1981). In this research the cold seawater (5℃) is pumped from about 500 m depth and 5 km from the shore and passes through an onshore heat exchanger field to condense the water vapor of the atmospheric air. The results show that the scheme is not economically suitable due to high pumping power. Gandhidasan and Abualhamayel (2005) developed a mathematical model, based on the energy balance equations to find the condensation rate from the atmospheric air. Habeebullah (2009) developed a new model in which moist-air was cooled over evaporator coils of refrigeration machines for water extraction in hot humid regions.

In humid regions, atmospheric air (moist-air) usually includes a considerable amount of water vapor. Under the expansion processes, say through nozzles, the steam portion of the moist-air can condense and a second phase (liquid phase) forms. Computation of compressible moist-air flows through nozzles and other geometries using equilibrium thermodynamic model, have been studied by Hamidi and Kermani (2013a, 2013b), who compared the content of condensate generation in moist-air case with that of pure steam. It has been observed that the content of wetness at nozzles exit in the case of moist-air is more than that of pure steam under similar operating conditions. The reason is due to the internal flow of heat from steamportion toward air that accelerates the steam condensation rate. In this paper a numerical study of water production from atmospheric air in geographically humid regions is performed.

1.1 Problem Definition

The atmospheric moist-air is accelerated through a converging-diverging nozzle, and is discharged to a liquid/gas separating chamber, in which liquid water is collected from the bottom of the chamber, and a compressor and motor-pump assembly is installed at the top of the chamber to produce the required vacuum pressure of about 30 kPa (abs). Figure 1 shows the schematic of the apparatus. The results show that, the energy consumed by the compressor for production 1 kg of water will be 1.279 kWh. The price of 1 kWh is 372 Rials, therefore the price for the production of 1 kg liquid water will be 475.8 Rials, therefore, the scheme is economically suitable. The present computation is under the isentropic operation of the nozzle, since all of the aerodynamic and thermodynamic losses (see Kermani and Gerber,(2003)), have not been included in the present study.

The present study is at its preliminary stages that provide a basis for the design and make of such a system to produce water from atmospheric-air. Some of the issues that will be addressed in future studies include the separation mechanisms of the liquid water from the gas phase and the shape of the downstream chamber. Computational domain used in the present study is a converging-diverging nozzle shown in Fig. 1.

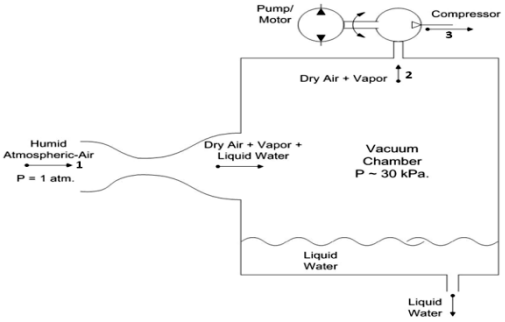

Fig. 1. Schematic of water production facility.

In the present study, parametric studies are performed for the atmospheric-air conditions, 40℃ ≤ T ≤ 50℃and relative humidity, 49.6%≤ Ø ≤100%. For these range of operating conditions and nozzle D (see Fig. 2), chosen from the Moore *et al*. (1973) paper having the area ratio of A_{exit}/A_{throat} = 1.17 , the liquid mass flow rates falls in the range 0.272 to 0.376 kg/s.

1.2 Detail of the Present Numerical Algorithm

The continuity, momentum and energy equations have been written in a fully conservative form for quasi one-dimensional flow through a converging-diverging nozzle. The gas portions of the two-phase mixture (water vapor + dry air) are assumed to obey the ideal gas equation of state. The flow is assumed to obey equilibrium thermodynamic model. The governing PDEs for both pure steam and moist-air are numerically solved. The detail of the numerical solution for the condensation of pure steam is given by Kermani *et al*. (2006), so they are not repeated here. The third-order upwind biased scheme of Roe (1981) has been used for spatial discretization, while for temporal integration the Lax-Wendroff second order scheme is implemented. The spurious numerical oscillations in the present high resolution computations are damped using the van Albada flux limiter (1982). The expansion shocks have also been avoided using the entropy correction formula given by Kermani and Plett (2001).

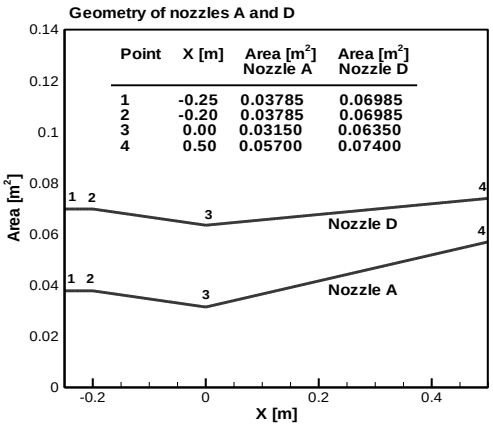

Fig. 2. Geometry of two different nozzles (A) and (D) taken from Moore *et al*. (1973) paper.

2. GOVERNING EQUATIONS

The governing equations for quasi one-dimensional, unsteady, inviscid and compressible flows are composed of the conservation laws of continuity, momentum and energy, and are shown in full conservative form. In the absence of body forces one can write (Hoffmann and Chiang, (1993)):

$$\frac{\partial Q}{\partial t}+\frac{\partial F}{\partial x}+H=0, \tag{1}$$

$$Q=A\begin{bmatrix}\rho\\ \rho u\\ \rho e_t\end{bmatrix}, F=A\begin{bmatrix}\rho u\\ P+\rho u^2\\ \rho u h_t\end{bmatrix},\ H=\begin{bmatrix}0\\ -P\dfrac{dA}{dx}\\ 0\end{bmatrix}. \tag{2}$$

Here $Q, F$and $H$are respectively, the conservative vector, the flux vector and the source term.A is the cross-sectional area of the nozzle, $\rho$is the mixture density(= $\rho_{mix}=\rho_s+\rho_a$, where ρ_s and ρ_a are the density of the steam (vapor + liquid) and air respectively) and $u$is the velocity. In this study the slip velocity between the gas and the liquid phases is ignored. This is a reasonable assumption that will be explained in detail in results. In Eqn. (2), $P$is the mixture pressure (= $P_{mix}=P_v+P_a$, where $P_v$and P_a are the vapor and air pressures respectively). For the present low pressure computation, the ideal gas equation of state is of sufficient accuracy, hence:

$$P_a=\rho_a R_a T, \qquad R_a=287\ \text{J/kg.K},$$

$$P_v=\rho_v R_v T, \qquad R_v=461.4\ \text{J/kg.K}. \tag{3}$$

Here, $\rho_a$and ρ_v are the density of the air and vapor respectively. In wet regions, if the volume of liquid phase is ignored (this is a correct assumption whose accuracy will be discussed later in detail in results), one can write, $\rho_s=\rho_v/\chi$, where χ is the

quality of the steam. It is noted that in this study the steam is referred to the mixture of liquid water and vapor.e_t and h_t are respectively the total internal energy and total enthalpy of the mixture (steam + air):

$$e_t = \frac{\dot{m}_a}{\dot{m}_{mix}} e_a + \frac{\dot{m}_s}{\dot{m}_{mix}} e_s + \frac{u^2}{2}, \dot{m}_{mix} = \dot{m}_s + \dot{m}_a, \tag{4}$$

$$h_t = e_t + P/\rho. \tag{5}$$

The humidity ratio of the moist-air $(\omega)$is defined as:

$$\omega = \dot{m}_v/\dot{m}_a, \tag{6}$$

where $\dot{m}_v$, is the mass flow rate of the vapor (the dry portion of the steam) and $\dot{m}_a$ is the mass flow rate of the dry air. Up to the condensation onset, the humidity ratio along the nozzle remains constant which is equal to humidity ratio of the reservoir:

$$\omega_{res} = \dot{m}_v/\dot{m}_a = \dot{m}_s/\dot{m}_a = constant. \tag{7}$$

Up to the condensation onset, $\dot{m}_s = \dot{m}_v$, beyond the condensation onset,$\dot{m}_v < \dot{m}_s$,since the steam is condensed and second phase (liquid) is formed, therefore the mass flow rate of vapor $(\dot{m}_v)$is reduced. The enthalpy of evaporation (h_{fg}) of the steam portion is obtained from:

$$h_{fg} = e_{fg} + R_v.T, \tag{8}$$

where $e_{fg}$is the latent internal energy. A second-order polynomial can accurately represent the relationship between $e_{fg}$and T,and the coefficients are provided by Kermani *et al*. (2006). The internal energy of the vapor and air, respectively,$e_v$and $e_a$are determined by assuming a constant value for the specific heats:

$$e_v = c_{v,v}.T, c_{v,v} = R_v/(\gamma_v - 1), \gamma_v = 1.32, \tag{9}$$

$$e_a = c_{v,a}.T, c_{v,a} = R_a/(\gamma_a - 1), \gamma_a = 1.4. \tag{10}$$

Equation (9) can be used to obtain the saturated liquid internal energy:

$$e_f = e_g - e_{fg}, \qquad e_g = c_{v,v}.T_{sat}. \tag{11}$$

In dry regions the internal energy of the steam is obtained from, $e_s = e_v = c_{v,v}.T$, while in wet regions:

$$e_s = e_f + \chi e_{fg}. \tag{12}$$

Substituting Eqs. (7) and (12) in Eqs. (4) and (5), the total internal energy and total enthalpy of the mixture (moist-air) in wet regions are obtained as follows:

$$e_t = \frac{1}{1+\omega_{res}} e_a + \frac{\omega_{res}}{1+\omega_{res}}\left(e_f + \chi e_{fg}\right) + \frac{u^2}{2}, \quad e_a = c_{v,a}.T, \tag{13}$$

$$h_t = \frac{1}{1+\omega_{res}} e_a + \frac{\omega_{res}}{1+\omega_{res}}\left(e_f + \chi e_{fg}\right) + \frac{u^2}{2} + \frac{P}{\rho}. \tag{14}$$

In this study, the entropy of the flow is computed in a similar manner that applied for internal energy and enthalpy. The entropy of air is obtained using the temperature and partial pressure of air:

$$s_a = c_{p,a} lnT - R_a lnP_a, \quad c_{p,a} = \gamma_a R_a/(\gamma_a - 1). \tag{15}$$

Similarly, the entropy of the steam portion in dry regions is obtained using the temperature and partial pressure of vapor:

$$s_s = s_v = c_{p,v} lnT - R_v \, l \, n \, P_v, \; c_{p,v} = \gamma_v R_v/(\gamma_v - 1), \tag{16}$$

while in wet regions:

$$s_s = s_f + \chi s_{fg}, \qquad s_{fg} = h_{fg}/T,$$
$$s_g = c_{p,v} lnT - R_v lnP_v, \qquad s_f = s_g - s_{fg}. \tag{17}$$

Finally the total entropy of the mixture (moist-air) is obtained as follows:

$$s_t = s_{mix} = \frac{\dot{m}_a}{\dot{m}_{mix}} s_a + \frac{\dot{m}_s}{\dot{m}_{mix}} s_s = \frac{1}{1+\omega_{res}} s_a + \frac{\omega_{res}}{1+\omega_{res}} s_s. \tag{18}$$

3. NUMERICAL SOLUTION

3.1 Time and Space Discretization

For the time discretization, an explicit two-step predictor-corrector scheme has been used to march the solution from time level $n$to $n+1$ (Tannehill *et al*. (1997)):

$$Q_i^{n+\frac{1}{2}} = Q_i^n - 0.5 \frac{\Delta t}{\Delta x}\left(F_{E,i}^n - F_{W,i}^n\right) - 0.5 \, \Delta t \, H_i^n, \tag{19}$$

where, i corresponds to any arbitrary internal nodal, and $F_{E,i}^n$ and $F_{W,i}^n$ are the numerical fluxes evaluated at the east $(E)$and west (W) faces of the control volume (Tannehill *et al*. (1997)):

$$F_{E,i} = \frac{1}{2}\left(F_{E,i}^R + F_{E,i}^L\right) - \frac{A_{E,i}}{2}\sum_{k=1}^{3}\left|\hat{\lambda}_{E,i}^{(k)}\right|\delta w_{E,i}^{(k)} \hat{T}_{E,i}^{(k)}, \tag{20}$$

$$F_{W,i} = F_{E,i-1}, \tag{21}$$

where λ, is the eigenvalue of the Jacobian flux matrix, T represents the corresponding eigenvector, $\delta w$is the wave amplitude vector and A is the cross-sectional area of the nozzle. In Eqn. (20), k corresponds to each wave propagating in the$x-t$domain. The predictor step is followed by the corrector step, which gives a central difference around $n+1/2$:

$$Q_i^{n+1} = Q_i^n - \frac{\Delta t}{\Delta x}\left(F_{E,i}^{n+\frac{1}{2}} - F_{W,i}^{n+\frac{1}{2}}\right) - \Delta t H_i^{n+\frac{1}{2}}. \quad (22)$$

For the spatial discretization, a third order upwind-biased with a MUSCL extrapolation strategy (van Leer,(1979)) is applied to obtain the primitive variable at the left (L) and the right(R)sides of the cell faces. In this approach, the nodal values are extrapolated to the L and Rcell faces to obtain the Roe (1981)averaged conditions. Various parameters are used in the literature for extrapolation purposes, (Thomas and Walters, (1987)), including the elements of the conservative vector Q, the primitive variables P, ρ, T, u,etc. We use the primitive variables $P, T$and$u$in dry regions, but it is noted that pressure and temperature are not independent in wet regions, so the quality $(\chi)$is extrapolated to the cell faces instead of pressure in wet regions. The local pressure of steam in the wet regions is determined from the saturated pressure at the local mixture temperature (Khakbaz Baboli and Kermani, (2008)). The following third-order extrapolation scheme is used here:

$$q_{E,i}^L = q_i + \frac{1}{4}[(1-k_0)\Delta_W q_i + (1+k_0)\Delta_E q_i], \quad (23)$$

$$q_{E,i}^R = q_{i+1} - \frac{1}{4}[(1-k_0)\Delta_{EE} q_i + (1+k_0)\Delta_E q_i], \quad (24)$$

$$\Delta_W q_i = q_i - q_{i-1}, \Delta_E q_i = q_{i+1} - q_i, \Delta_{EE} q_i = q_{i+2} - q_{i+1}, \quad (25)$$

where $q \in (P, T, u)$in dry regions, while in wet regions $q \in (T, u, \chi)$. The third-order upwind biased scheme corresponds to a choice of $k_0 = 1/3$ in Eqs. (23) and (24). Spurious numerical oscillations that are unavoidable in high resolution computations are prevented using the van Albada flux limiter (1982):

$$q_{E,i}^L = q_i + \frac{\emptyset_i}{4}[(1-k_0)\Delta_W q_i + (1+k_0)\Delta_E q_i], \quad (26)$$

$$q_{E,i}^R = q_{i+1} - \frac{\emptyset_{i+1}}{4}[(1-k_0)\Delta_{EE} q_i + (1+k_0)\Delta_E q_i], \quad (27)$$

where the limiter function $\phi_i$depends on forward and backward differences according to:

$$\emptyset_i = \frac{2(\Delta_W q_i)(\Delta_E q_i) + \varepsilon_0}{(\Delta_W q_i)^2 + (\Delta_E q_i)^2 + \varepsilon_0}, \quad \varepsilon_0 = 0^+. \quad (28)$$

Roe's scheme incorrectly captures expansion shocks in the regions where eigenvalues of the Jacobian matrix of flux vector vanish. To avoid expansion shocks from appearing we use a previously developed algorithm which given by Kermani and Plett (2001).

3.2 Roe's Averaging for Moist-air Computation

The numerical fluxes F_E and F_W of the Roe's scheme is calculated at the so-called Roe-averaged conditions obtained from the L and R states on both sides of a cell face. In this paper the results of an earlier computation of the Roe scheme to the two-phase pure steam flow (Kermani *et al*., (2006)), is extended for moist-air flow applications. It is proposed that density and total enthalpy at the Roe-averaged condition to be obtained based on the properties of the mixture (steam + air) at the sides of the cell face:

$$\hat{\rho}_E = \sqrt{\rho_E^L \rho_E^R}, \ \left(\hat{h}_t\right)_E = \left(\sqrt{\rho_E^L}(h_t)_E^L + \sqrt{\rho_E^R}(h_t)_E^R\right) \Big/ \left(\sqrt{\rho_E^L} + \sqrt{\rho_E^R}\right), \quad (29)$$

where the density and enthalpy of the moist-air in wet regions are determined from:

$$\rho_E^L = (\rho_a)_E^L + (\rho_s)_E^L = (\rho_a)_E^L + (\rho_v)_E^L/(\chi)_E^L, \quad (30)$$

$$(h_t)_E^L = \frac{1}{1+\omega_{res}}(e_a)_E^L + \frac{\omega_{res}}{1+\omega_{res}}\left((e_f)_E^L + \chi_E^L\left(e_{fg}\right)_E^L\right) + \frac{((u)_E^L)^2}{2} + \frac{P_E^L}{\rho_E^L}. \quad (31)$$

The density of air(ρ_a) is determined from $\rho_a = P_a/(R_a T)$,while the density of the vapor in the wet regions is computed from, $\rho_v = P_{sat}/(R_v T)$, that $P_{sat}$is obtained vs. T (see Khakbaz Baboli and Kermani, (2008)).

3.3 Moisture Evaluation

The conservative vector (Q), at each time level provides values of $(Q_1, Q_2, Q_3) = (\rho A, \rho u A, \rho e_t A)$ where ρ,is the density of the moist-air (air + steam). Removing the density of the air portion from the mixture, the density of the steam can be determined. Then,$u$can be calculated from, $u = Q_2/Q_1$, and, $e_{mix} = e_t - u^2/2$. Now by removing the internal energy of the air portion from that of the mixture, the internal energy of the steam can be obtained. Finally, the thermodynamic state and moisture content (if present) can be determined using a trial and error process from two independent properties of steam, namely internal energy and density, e_s and ρ_s, respectively.

3.4 Boundary Conditions

In this study, two nozzle geometries (nozzles A and D) are taken from the Moore *et al*. (1973) paper. The geometries of these nozzles are shown in Fig. 2. The inflow is assumed to be subsonic, where the stagnation pressure $(P_{0,in})$,stagnation temperature $(T_{0,in})$and the humidity ratio of the reservoir$(\omega_{res})$are specified. At the inlet of the nozzle the flow properties have been determined from the following conditions: mixture pressure $(P_{mix.})$ and the steam quality $(\chi)$are extrapolated from the interior domain to the inlet face, and the isentropic condition from the upstream stagnation conditions to the inlet face is enforced. At the exit, the flow is supersonic in which all of the primitive variables are extrapolated from the interior domain.

4. VALIDATION AND RESULTS

4.1 Validation

For validation purposes two nozzle geometries are taken from the Moore *et al*. (1973) paper, namely, nozzles A and D, the geometry of which are shown in Fig. 2. Nozzle A of these series has the highest expansion rate while nozzle D possesses the lowest. Due to the availability of experimental data from the Moore *et al*. (1973) paper for pure steam, the accuracy assessment of the present computations is performed vs. these experimental data. Comparisons with the Moore *et al*. data are performed by two different solvers: (i) a pure steam solver and (ii) a moist-air solver in which the humidity ratio of the reservoir is set to a very large number, i.e. $\omega_{res} \rightarrow \infty$. The case (ii) corresponds to a pure steam case too and is expected to echo the same results as case (i). In the case (ii) ω_{res} is set to 1000. Figure 3 (a) shows the results of numerical solutions for pressure distribution along the Moore$_A$ and Moore$_D$ nozzles for both of the cases (i) and (ii) mentioned above. As shown in this figure, a good agreement between the results is obtained, where the maximum errors (deviation of the computed results from the experimental data) for Moore$_A$ and Moore$_D$ nozzles have been obtained as 12% and 10%, respectively. Also the wetness fraction profiles along the these nozzles for cases (i) and (ii) have also been compared with those of Kermani *et al*. (2006), and identical results were achieved, that is shown in Fig. 3 (b).

In the case of low humidity ratio, $\omega \rightarrow 0$ as the moist-air tends to dry air, the shock tube data is used to validate our numerical solution (not shown here). The results show that (see Hamidi and Kermani 2013a, 2013b), an excellent agreement between the numerical results and exact solution is obtained. Therefore, the numerical method which is proposed in this paper is capable to simulate compressible flow problems with satisfactory precision.

4.2 Results

Sample of the computed results are shown in this section. We limit the results to Moore$_D$ nozzle, but similar results for other nozzles can also be obtained. Figure 4, (a) and (b) show, respectively, the profiles of wetness fractions, and liquid mass flow rates along the Moore$_D$ nozzle for both pure steam and moist-air flows. In the case of moist-air the nozzle inflow stagnation conditions were taken as $T_{0,in}$=323.15 K (50℃) and $P_{0,in}$= 1 atm, where the computations were performed at two ω_{res} = 0.086 and 0.04, while pure steam computations were performed at $T_{0,in}$=323.15 K, $P_{0,in}$= 0.122 and 0.0604 atm. It is noted that to be able to correctly compare the moist-air and pure steam results, the stagnation pressure of steam at the nozzle inlet in the case of pure steam is adjusted to the stagnation partial pressure of steam in the moist-air cases. That is, the stagnation partial pressure of steam ($P_{0,v}$), in moist-air case is first calculated then it is set to the stagnation pressure of pure steam at the nozzle inlet. Using this terminology, for the case of moist-air with ω_{res} = 0.086, $P_{0,v}$ is determined as 0.122 atm, and similarly for ω_{res} = 0.04, $P_{0,v}$ = 0.0604 atm.

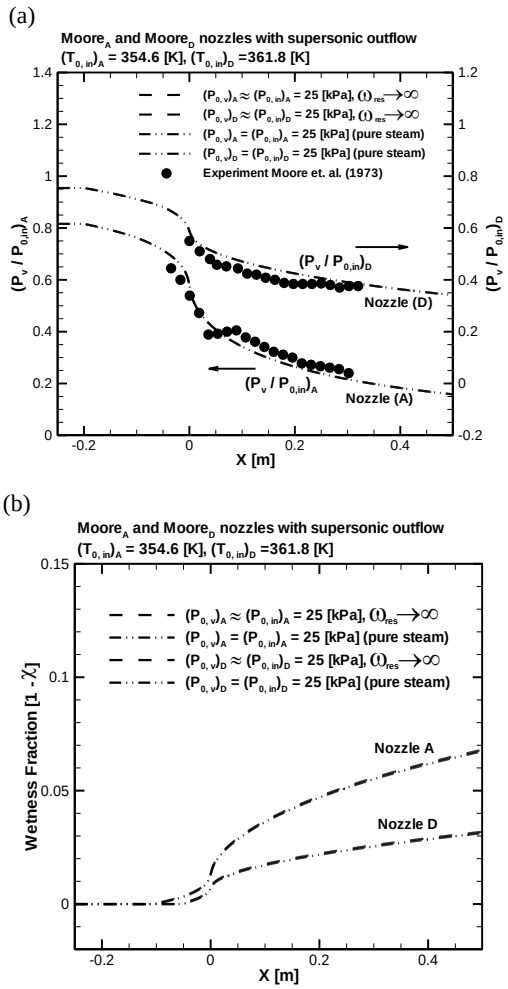

Fig. 3. Comparisons of pressure (a) and wetness fraction (b) distributions along Moore$_A$ and Moore$_D$ nozzles for moist-air in the case of, $\omega_{res} \rightarrow \infty$, and pure steam.

As shown in Fig. 4, the wetness fraction and liquid mass flow rate of moist-air case are much higher than those of pure steam. This is due to the fact that the specific heat of steam is greater than that of air hence there will be a local reversible removal of heat from steam toward the air. As a result, in the moist-air case the wetness fraction and liquid mass flow rate at the nozzle exit are much higher. For example, as shown in Fig. 4 (a) in the case of moist-air flow with, $\emptyset = 100\%$, wetness fraction 35.96% at the nozzle exit is achieved. Similarly, in the case of moist-air with $\emptyset = 100\%$ the condensate production rate, $\dot{m}_l$, at the nozzle exit is 0.376 kg/s, as shown in Fig. 4 (b). While in the case of pure steam at similar conditions ($T_{0,in}$=323.15 K, $P_{0,in}$= 0.122 atm) wetness fraction 4.66% and $\dot{m}_l$ = 0.06 kg/s were obtained at the nozzle exit. That is, 6.27 times more condensate is produced in the case of moist-air.

(a)

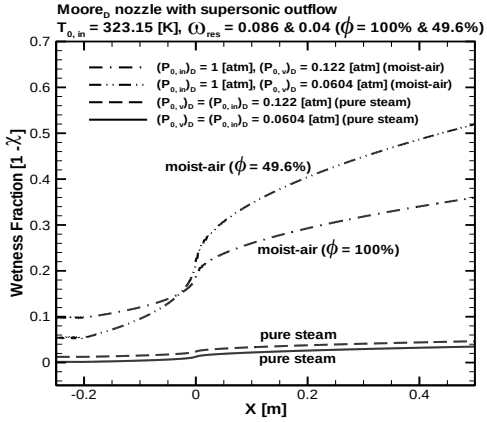

(b)

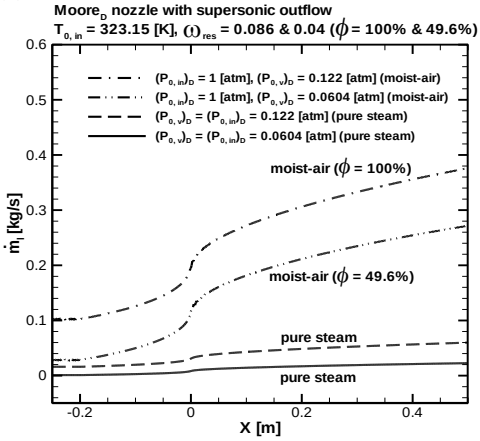

Fig. 4. Comparisons of wetness fraction (a) and liquid mass flow rate (b) profiles along Moore$_D$ nozzle, for isentropic expansion of pure steam and moist-air with the similar stagnation pressure of the steam portion at the nozzle inlet.

It is important to emphasize that, although the wetness fraction determined in the moist-air conditions at most can even reach 50%, but as the ratio of $\dot{m}_l/\dot{m}_{mix}$ is in the order of 2 to 3.5% (see Fig. 5 as an example), therefore the volume fraction of the liquid water to that of the mixture remain negligible. Hence the no-slip condition between the gas and liquid phases will still remain valid. Figure 5 represents the mass flow rates of the liquid and gas species along the nozzle at the conditions, $T_{0,in}$= 323.15 K, $P_{0,in}$= 1 atm and ω_{res} = 0.08 ($\emptyset$ = 93.5%). As shown in this figure $\dot{m}_{mix}$ $(= \dot{m}_a + \dot{m}_s)$, $\dot{m}_a$ and $\dot{m}_s (= \dot{m}_v + \dot{m}_l)$ have been computed as constant along the nozzle, indicating that at the converged state the mass conservation of these species are well governed. On the other, along the nozzle and due to condensation, the mass flow rate of the liquid water ($\dot{m}_l$) is increased with the same rate (in magnitude) as water vapor is reduced. Also as shown in Fig. 5, $\dot{m}_s = 0.978$ kg/sand $\dot{m}_a =$ 12.22 kg/s, we determine $\omega_{res} = \dot{m}_s/\dot{m}_a = 0.978$ / 12.22 = 0.08, which is correctly retrieving the initially set reservoir humidity ratio $\omega_{res} = 0.08$. This is a self-consistency check of the solution. Also from the computed values of Fig. 5, $\dot{m}_{mix}$ = 13.2 kg/s, and at the nozzle exit $\dot{m}_l = 0.366$ kg/s and $\dot{m}_v = 0.612$ kg/sare obtained. Hence $\dot{m}_l/\dot{m}_{mix}$ = 0.366/13.2 = 0.0277, which is pretty consistent with the assumptions that the volume fraction of the liquid water to that of the mixture is negligible, and the no-slip condition between the gas and liquid phase.

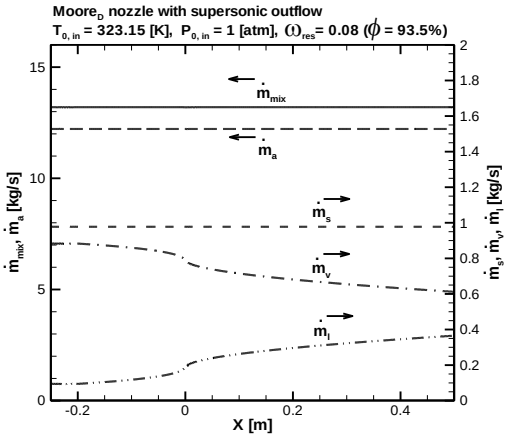

Fig. 5. Mass flow rate profiles of air portion $(\dot{m}_a)$, steam portion $(\dot{m}_s = \dot{m}_v + \dot{m}_l)$ and moist-air mixture $(\dot{m}_{mix} = \dot{m}_s + \dot{m}_a)$ along the Moore$_D$ nozzle for supersonic outflow.

Figure 6 shows the *T-s* diagram for the expansion of moist-air and its components along the nozzle. As shown in this figure the moist-air (air + steam) undergoes an isentropic expansion ($s_{mix} = constant$), while the components (air and steam) experience non-isentropic processes due to the reversible heat exchange between the phases. The direction of heat is from the steam with higher specific heat toward air with lower specific heat. As a result of the internal heat removal from the steam, the entropy of steam(s_s)decreases and the entropy of the air (s_a) increases along the nozzle. Quantitative values of temperature-entropy are also included in this figure for comparison purposes.

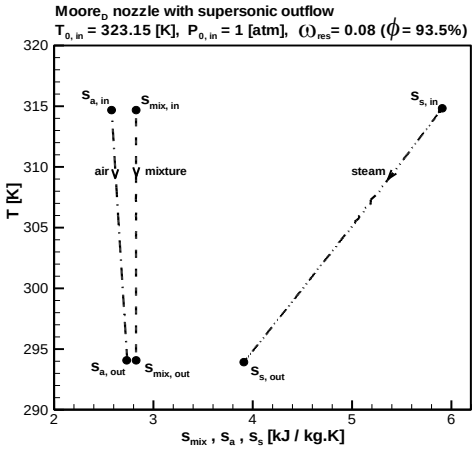

Fig. 6. *T-s* diagram for the isentropic expansion of the moist-air mixture along the Moore$_D$ nozzle, the mixture undergoes an isentropic expansion while due to internally reversible heat exchange between the air and steam the species experience non-isentropic processes.

Figure 7 (a) and (b), respectively, represent a

parametric study to illustrate the influence of inflow humidity ratio (relative humidity) on wetness fraction and water production rate along the nozzle. As shown in Fig. 7 (a) by increasing the humidity ratio the wetness fraction at the nozzle exit decreases, since by increasing the humidity ratio the mass fraction of air reduces. As a result the capacity of air as the recipient source of heat from the steam portion reduces too. On the influence on the rate of water production, by increasing the humidity ratio the water production rate increases, since the mass fraction of steam portion of the moist-air mixture increases.

(a)

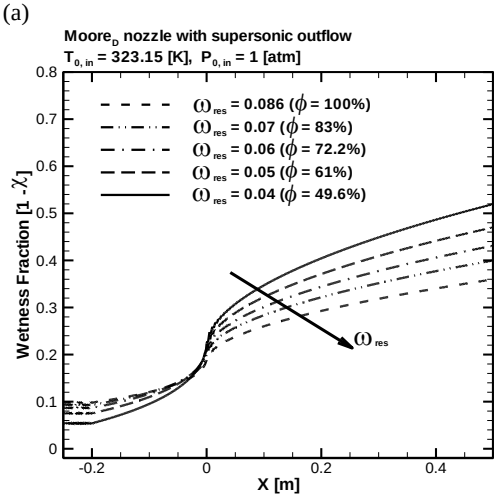

(b)

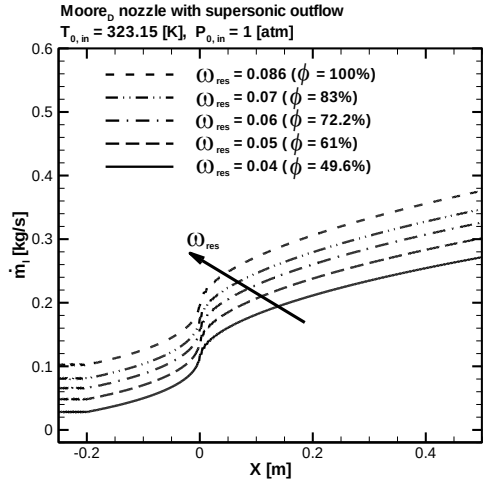

Fig. 7. The influence of humidity ratio on the wetness fraction (a) and liquid mass flow rate (b) profiles along the Moore$_D$ nozzle, for isentropic expansion of moist-air.

Table 1 summarizes the results of the parametric studies performed in this research. It shows the mass flow rate of water produced at the nozzle exit which shown in Fig. 1. For the range of atmospheric-air conditions $40°C \leq T \leq 50°C$and relative humidity $49.6\% \leq \emptyset \leq 100\%$, and the Moore$_D$ nozzle with area ratio of A_{exit}/A_{throat} = 1.17, the mass flow rate of water falls in the range 0.272 to 0.376 kg/s. The highest rate of 0.376 kg/s corresponds to the saturated-air state ($\emptyset = 100\%$).

Table 1 Summary of the results; the mass flow rate of water at the Moore$_D$ nozzle exit at ambient pressure 1 atm and prescribed temperature and humidity ratio

Case #	T_0	ω_{res} (Ø%)	$\dot{m}_l$(kg/s)
1	323.15 K	0.086 (100)	0.376
2	323.15 K	0.080 (93.5)	0.366
3	323.15 K	0.070 (83.0)	0.347
4	323.15 K	0.060 (72.2)	0.326
5	323.15 K	0.050 (61.0)	0.302
6	323.15 K	0.040 (49.6)	0.272
7	318.15 K	0.065 (100)	0.360
8	318.15 K	0.060 (92.9)	0.348
9	318.15 K	0.055 (85.8)	0.336
10	318.15 K	0.050 (78.6)	0.323
11	318.15 K	0.045 (71.3)	0.307
12	318.15 K	0.040 (63.8)	0.291
13	313.15 K	0.049 (100)	0.340
14	313.15 K	0.045 (92.6)	0.328
15	313.15 K	0.040 (82.9)	0.310

4.3 Sample Calculation and Feasibility Study for Desalination Application

As an application for the present study, desalination of liquid water from moist air in highly humid regions is considered. As a sample calculation the content of 1 kg produced liquid water and consumed energy is determined. Applying the first law of thermodynamics around the compressor (see Fig. 1), we can write:

$$\dot{Q}_{c.v} - \dot{W}_{c.v} = \sum \dot{m}_e \left(h_e + \frac{V_e^2}{2} + gZ_e\right) - \sum \dot{m}_i \left(h_i + \frac{V_i^2}{2} + gZ_i\right) \quad (32)$$

We assume that changes in kinetic and potential energy are negligible and the compressor to be adiabatic:

$$\left|\dot{W}_{2-3}\right| = \dot{m}_{2-3} C_{p,mix} \left(T_{3,s} - T_2\right) / \eta_{s,c} \quad (33)$$

Where $\eta_{s,c}$ is the compressor isentropic efficiency, taken as 0.85. This calculation is performed for nozzle D with 10 cm^2 throat cross section and inlet atmospheric condition: $T_{0,in}$= 323.15 K, $P_{0,in}$= 1 atm and $\emptyset = 93.5\%$. The noted atmospheric condition corresponds to Case # 2 in Table 1. It is noted that the mass flow rate of the components (air, vapor and liquid) are given in Fig. 5. The specific heats ($C_{p,mix}, C_{v,mix}$) and the specific heat ratio (γ_{mix}) of the dry air and vapor (step 2 to 3 in Fig. 1), are determined by:

$$C_{p,mix} = \sum_{i=1}^{2} C_i C_{p,i} = \frac{0.612}{12.22 + 0.612} \times 1.872 + \frac{12.22}{12.22 + 0.612} \times 1.004 = 1.0454\ kJ/kg.K$$

$$C_{v,mix} = \sum_{i=1}^{2} C_i C_{v,i} = \frac{0.612}{12.22 + 0.612} \times 1.41 + \frac{12.22}{12.22 + 0.612} \times 0.717 = 0.75\ kJ/kg.K \quad (34)$$

$$\gamma_{mix} = C_{p,mix}/C_{v,mix} = 1.394,$$

Where C_i is the mass fraction of the vapor or air. At the compressor inlet (nozzle exit), $P_2 = 33.82\ kPa$, $T_2 = 293.9$ (see Fig. 6) and at the compressor outlet, $P_3 = 101.325\ kPa$. For the ideal, isentropic process from 2→ 3 in Fig. 1, we can write:

$$\frac{T_{3,s}}{T_2} = \left(\frac{P_3}{P_2}\right)^{\frac{\gamma_{mix}-1}{\gamma_{mix}}} \rightarrow \frac{T_{3,s}}{293.9} = \left(\frac{101.325}{33.82}\right)^{\frac{1.394-1}{1.394}} \rightarrow T_{3,s} = 400.7K. \quad (35)$$

The mass flow rate of the dry air and vapor (step 2 to 3 in Fig. 1) for 10 cm^2 throat cross section is determined by:

$$\dot{m}_{2-3} = \underbrace{12.832\,(kg/s)}_{\substack{\text{mass flow rate of dry air and vapor } (\dot{m}_v + \dot{m}_a) \text{ for nozzle throat} \\ \text{area } 635cm2}} \underbrace{\frac{10\,cm^2}{635\,cm^2}}_{\text{Area ratio}} = 0.2021\,kg/s \quad (36)$$

Therefore the power consumed by the compressor will be:

$$\left|\dot{W}_{2-3}\right| = 0.2021 \times 1.0454 \times \frac{(400.7 - 293.9)}{0.85} = 26.55\ kW. \quad (37)$$

The mass flow rate of the liquid water is:

$$\dot{m}_l = \underbrace{0.366\,(kg/s)}_{\substack{\text{liquid mass flow rate} \\ (\dot{m}_l) \text{ for nozzle throat} \\ \text{area } 635cm2}} \underbrace{\frac{10\,cm^2}{635\,cm^2}}_{\text{Area ratio}} = 0.005764\,kg/s \quad (38)$$

Therefore the time for production of 1 kg water is:

$$t = \frac{1}{0.005764} = 173.5\ sec. \quad (39)$$

The energy consumed by the compressor for production 1 kg of water will be:

$$W_{comp} = 26.55 \times \frac{173.5}{3600} = 1.279\ kWh \quad (40)$$

The price of 1 kWh is 372 Rials, therefore the price for the production of 1 kg liquid water (almost 1 Lit.) will be:

$$Price = 1.279\ kWh \times 372\ Rials = 475.8\ Rials. \quad (41)$$

These results show that the scheme is economically suitable.

5. CONCLUSION

Condensation phenomena for flows of pure-steam and moist-air through converging-diverging nozzles are numerically studied. The main focus was on the fluid mechanics of the flow and the rates of the liquid condensate (water) produced. The task is performed using a high resolution flux difference splitting scheme of Roe (1981) with a spatially third order and temporally second order accurate algorithm. The flow is assumed to obey equilibrium thermodynamic model. In order to assess the accuracy of the present computations the results are compared with the experimental data of Moore *et al*. (1973) for pure steam case ($\omega_{res} \rightarrow \infty$). Comparisons show good agreement between the results. The following conclusions can be drawn:

1. For the isentropic process of moist-air studied here, it is observed that each of the species, steam and air experience non-isentropic processes due to the heat flow from a species with higher specific heat value (steam) toward the other species with lower specific heat value (air here).
2. As a result of item 1 above, in the case of moist-air, the content of wetness at the nozzle exit becomes much higher than that of pure steam case.
3. The idea mentioned in items 1 and 2 above can be generalized as follows. When the mixture of steam and an additive gas of lower specific heat values (like air, carbon dioxide, oxygen or an appropriate combination of them) are used to produce liquid water condensate, the content of liquid water at the nozzle exit can be much higher than the case of pure steam. In the present study, the additive gas is dry air with mixture being atmospheric-air in hot and humid climates.
4. The results show that, the energy consumed by the compressor for production 1 kg of water will be 1.279 kWh. The price of 1 kWh is 372 Rials, therefore the price for the production of 1 kg liquid water will be 475.8 Rials. These results show that the scheme is economically suitable.
5. Future Work: As described in this study, in the case of moist-air, a significantly higher condensate is generated, but, the separation mechanisms of the liquid water from the gas phase and the shape of the downstream chamber should be studied.

REFERENCES

Gandhidasan, P. and H. I. Abualhamayel (2005). Modeling and testing of a dew collection system. *Desalination* 180, 47–51.

Habeebullah, B. A. (2009). Potential use of evaporator coils for water extraction in hot and

humid areas. *Desalination* 237, 330–345.

Hamidi, S. and M. J. Kermani (2013). High resolution computation of compressible condensing/evaporating moist-air flow for external and internal flows. *The Aeronautical Journal* 117, 427-444.

Hamidi, S. and M. J. Kermani (2013). Numerical solution of compressible two-phase moist-air flow with shocks. *European Journal of Mechanics - B/Fluids* 42, 20-29.

Hoffmann, K. A. and S. T. Chiang (1993). *Computational Fluid Dynamics for Engineers, Vol. II*, Engineering Education Systems, Wichita, Kansas, USA.

Kermani, M. J. and A. G. Gerber (2003). A general formula for the evaluation of thermodynamic and aerodynamic losses in nucleating steam flow. *Int. J. of Heat and Mass Transfer* 46, 3265–3278.

Kermani, M. J. and E. G. Plett (2001). Modified Entropy Correction Formula for the Roe Scheme 2001-0083.

Kermani, M. J., A. G. Gerber and J. M. Stockie (2006). An Application of Roes High Resolution Scheme to Transonic Two-Phase Flow through Nozzles. *Iranian Journal of Mechanical Engineering: Transaction of the ISME* 7 (1), 60-77.

Khakbaz Baboli, M. and M. J. Kermani (2008). A two-dimensional, transient, compressible isothermal and two-phase model for the air-side electrode of PEM fuel cells. *Electrochimica Acta* 53, 7644–7654.

Moore, M. J., P. T. Walters, R. I. Crane and B. J. Davidson (1973). *Predicting the fog drop size in wet steam turbines*, Institute of Mechanical Engineers (UK), Wet Steam 4 Conf., University of Warwick 37/73.

Rajvanshi, A. K.(1981). Large scale dew collection as a source of fresh water supply. *Desalination* 36, 299–306.

Roe, P. L. (1981). Approximate Riemann Solvers, Parameter Vectors and Difference Schemes. *J. Comput. Phys.* 43, 357-372.

Tannehill, J. C., D. A. Andersonand and R. H. Pletcher (1997). *Computational Fluid Mechanics and Heat Transfer*, second edition.

Thomas, J. L. and R. W. Walters (1987). Upwind Relaxation Algorithms for Navier-Stokes Equations 25, 527-537.

Van Albada, G. D., B. van Leer and W. W. Roberts (1982). A Comparative Study of Computational Methods in Cosmic Gas Dynamics. *Astron. Astrophys.* 108, 76-84.

Van Leer, B.(1979). Towards the Ultimate Conservation Difference Scheme, A Second Order Sequel to Godunov's Method. *J. Comput. Phys*. 32, 110-136.

Wahlgren, R. V. (2001). Atmospheric water vapour processor designs for potable water production: A review. *Water Res* 35(1), 1–22.